Check for updates

Chemistry–A European Journal
Research Article
doi.org/10.1002/chem.202301345
Chemistry Europe
European Chemical Societies Publishing
www.chemeurj.org

Room-Temperature Solid-State Polymer Electrolyte in Li-$LiFePO_4$, Li-S and Li-O_2 Batteries

Vittorio Marangon,[a, b] Luca Minnetti,[b] Edoardo Barcaro,[a] and Jusef Hassoun*[a, b, c]

Abstract: A solid polymer electrolyte has been developed and employed in lithium-metal batteries of relevant interest. The material includes crystalline poly(ethylene glycol)dimethyl ether (PEGDME), LiTFSI and $LiNO_3$ salts, and a SiO_2 ceramic filler. The electrolyte shows ionic conductivity more than 10^{-4} S cm^{-1} at room temperature and approaching 10^{-3} S cm^{-1} at 60 °C, a Li^+-transference number exceeding 0.3, electrochemical stability from 0 to 4.4 V vs. Li^+/Li, lithium stripping/deposition overvoltage below 0.08 V, and electrode/electrolyte interphase resistance of 400 Ω. Thermogravimetry indicates that the electrolyte stands up to 200 °C without significant weight loss, while FTIR spectroscopy suggests that the LiTFSI conducting salt dissolves in the polymer. The electrolyte is used in solid-state cells with various cathodes, including $LiFePO_4$ olivine exploiting the Li-insertion, sulfur–carbon composite operating through Li conversion, and an oxygen electrode in which reduction and evolution reactions (i.e., ORR/OER) evolve on a carbon-coated gas diffusion layer (GDL). The cells operate reversibly at room temperature with a capacity of 140 mA h g^{-1} at 3.4 V for $LiFePO_4$, 400 mA h g^{-1} at 2 V for sulfur electrode, and 500 mA h g^{-1} at 2.5 V for oxygen. The results suggest that the electrolyte could be applied in room-temperature solid polymer cells.

Introduction

Lithium-metal batteries (LMBs) have been shown since late 1990s to be the most energetic rechargeable systems due to the extremely high gravimetric capacity of Li (3861 mA h g^{-1}) delivered at the lowest redox potential among the anodes (−3.040 V vs. standard hydrogen electrode).[1–4] Much effort has been devoted to stabilizing the lithium metal, including the formation of suitable solid electrolyte interphase (SEI) layers with high ionic conductivity, low electrochemical reactivity and relevant chemical stability.[5] However, the high energy content of Li metal can promote a relevant reactivity with large part of the liquid organic electrolytes leading to mechanical, chemical, and electrochemical instability of the SEI with final LMB failure.[6,7] The most suitable approach for an efficient use of Li in rechargeable battery involved the use of solid electrolytes, either polymeric or inorganic, instead of liquid ones in view of their mechanical stability and low flammability.[3,8] In particular, cells using polymer electrolytes based on poly(ethylene oxide) (PEO) with chemical formula $-(CH_2CH_2O)_n-$ and high molecular weight (>600 000 Da) demonstrated the most promising features in terms of scalability and practical applicability.[9–11] However, the mainly crystalline state at room temperature of high-molecular-weight PEO hinders suitable ionic conductivity for battery application, that is achieved only at temperature higher than 60 °C over which the polymer becomes predominantly amorphous.[12] Relevantly, a LMB using PEO-based electrolyte and $LiFePO_4$ (LFP) cathode with energy density higher than 100 W h kg^{-1} operating from 60 to 80 °C has been successfully launched onto the market as lithium metal polymer (LMP®) battery by the Bolloré Group (France).[13] A similar cell stability and scalability can be achieved at a temperature lower than 60 °C using the same Li-LFP configuration mentioned above, in which the PEO-based electrolyte is replaced by a solid poly(ethylene glycol)dimethyl ether (PEGDME) with low molecular weight (e.g., <5000 Da) for allowing suitable ionic conductivity and operative condition.[14] Recent results demonstrated the crucial role of PEGDME-based polymer electrolytes in stabilizing the electrochemical performance of lithium batteries using layered oxide-based cathodes such as $LiNi_{0.85}Co_{0.1}Mn_{0.05}O_2$ (NCM).[15] Following this trend, the energy density of the LMB can be remarkably increased by using cathodes with different chemistry rather than the olivine-structured LFP which relies on Li-(de)insertion electrochemical process.[16,17] Li-S and Li-O_2 batteries, based on the Li conversion reaction, have been suggested as the most promising candidates for increasing the energy density of the LMBs to values

[a] Dr. V. Marangon, E. Barcaro, Prof. J. Hassoun
University of Ferrara
Department of Chemical, Pharmaceutical and Agricultural Sciences
Via Fossato di Mortara 17, 44121, Ferrara (Italy)
E-mail: jusef.hassoun@iit.it
jusef.hassoun@unife.it
Homepage: https://docente.unife.it/jusef.hassoun
[b] Dr. V. Marangon, L. Minnetti, Prof. J. Hassoun
Graphene Labs, Istituto Italiano di Tecnologia
via Morego 30, Genova, 16163 (Italy)
[c] Prof. J. Hassoun
National Interuniversity Consortium of
Materials Science and Technology (INSTM)
University of Ferrara Research Unit, University of Ferrara
Via Fossato di Mortara, 17, 44121, Ferrara (Italy)

Supporting information for this article is available on the WWW under https://doi.org/10.1002/chem.202301345

© 2023 The Authors. Chemistry - A European Journal published by Wiley-VCH GmbH. This is an open access article under the terms of the Creative Commons Attribution License, which permits use, distribution and reproduction in any medium, provided the original work is properly cited.

© 2023 The Authors. Chemistry - A European Journal published by Wiley-VCH GmbH

15213765, 2023, 45, Downloaded from https://chemistry-europe.onlinelibrary.wiley.com/doi/10.1002/chem.202301345 by Universita Di Ferrara, Wiley Online Library on [08/10/2024]. See the Terms and Conditions (https://onlinelibrary.wiley.com/terms-and-conditions) on Wiley Online Library for rules of use; OA articles are governed by the applicable Creative Commons License

exceeding 300 W h kg^{-1}.[18] However, these triggering energy storage systems, mainly developed using liquid electrolyte, still suffer by the same severe issues affecting the LMB, that is, SEI instability, Li dendrites formation and cell failure with safety limits.[19,20] These emerging LMBs have additional critical issues that may affect the anode side, mainly related with the formation of reactive and nucleophilic intermediates during the electrochemical process, such as lithium polysulfides (Li_2S_x with $2 \leq x \leq 8$) in the Li-S battery or lithium peroxide (Li_2O_2) and superoxide (LiO_2) in the Li-O_2 one.[18,21–26] The use of polymer electrolyte, in analogy with the above reported LMB with insertion cathode, has been indicated as an adequate pathway to mitigate the issues of the lithium metal, in particular using the sulfur cathode.[27–30] Moreover, Li-O_2 and Li-S cells operating at room temperature have been reported using a plasticized or jellified version of the polymer electrolyte, able to conduct Li ions at lower temperature rather than the crystalline version of the same polymers.[31–35] However, the limited amount of reports on these interesting systems suggested further R&D for ensuring adequate energy density, efficiency, cycle life and scalability to a practical version for application in pivotal fields such as storage from renewable energy sources and electric vehicles (EVs).[36,37] In this work we have developed a composite polymer electrolyte (CPE) based on crystalline PEGDME including LiTFSI and $LiNO_3$ salts, and SiO_2 ceramic filler (indicated as PEGDME_CPE), treated with a liquid analogue solution of tetra(ethylene glycol)dimethyl ether (TEGDME_LE) subsequently removed to get a self-standing plasticized polymer electrolyte (indicated subsequently as PEGDME_PCPE).[38,39] A preliminary analysis has been conducted on the liquid TEGDME_LE solution by electrochemical impedance spectroscopy (EIS), chronoamperometry, linear sweep voltammetry (LSV), and cyclic voltammetry (CV). Furthermore, galvanostatic cycling (GC) on lithium metal cells with the liquid configuration have been performed exploiting LFP, sulfur, and oxygen cathodes. Subsequently, the PEGDME_PCPE electrolyte is fully characterized in terms of conductivity, lithium transference number, electrochemical and chemical stability using the techniques listed above. Thermogravimetric analysis (TGA) has been performed for investigating the electrolyte stability at high temperatures, while FTIR spectra have been collected to rationalize the involved chemical bonds. Polymer lithium cells using PEGDME_PCPE with LFP, S and O_2 cathodes have been assembled and galvanostatically cycled at room temperature to evaluate the applicability of the system. The results reported herein may allow the development of a new generation of LMBs exploiting the solid polymer configuration, characterized by a relevant safety and high energy content for future application in a variety of emerging fields.

Table 1. Ionic conductivity at infinite temperature (σ_∞), activation energy for ion conduction (E_a), and temperature of zero configurational entropy (T_0) for the PEGDME_LE according to VTF equation (1) used for the conductivity trend of Figure 1a . See the Experimental Section for acronyms and further details.

Electrolyte	σ_∞ [S cm^{-1}]	E_a [eV]	T_0 [K]
TEGDME_LE	$9.9\times10^{-3}\pm0.1\times10^{-3}$	$14.3\times10^{-3}\pm1.7\times10^{-3}$	221.2 ± 3.9

Results and Discussion

Prior to studying the PEGDME_PCPE, the liquid analogue TEGDME_LE is electrochemically characterized in Figure 1. The ionic conductivity trend reported vs. the temperature in Figure 1a (see corresponding Nyquist plots in Figure S1 in Supporting Information) shows the typical Vogel–Tamman–Fulcher (VTF) behavior, already observed for liquid glyme-based electrolytes, in particular at low temperatures.[40] Accordingly, the conductivity $\sigma(T)$ is plotted using the VTF Equation (1):

$$\sigma(T) = \sigma_\infty \exp\left(-\frac{E_a}{k_B(T-T_0)}\right) \quad (1)$$

where T_0 [K], also indicated as temperature of zero configurational entropy, is generally ~30 K lower than the glass transition temperature T_g [K] of the electrolyte.[41] The other parameters are the ionic conductivity at infinite temperature σ_∞ [S cm^{-1}], the activation energy for ion conduction E_a [eV], and the Boltzmann constant k_B (8.62 10^{-5} eV K^{-1}). Table 1 summarizes the results of the VTF plot for the TEGDME_LE.

The liquid electrolyte shows a conductivity ranging from 3×10^{-4} S cm^{-1} at 0 °C to 3×10^{-3} S cm^{-1} at 80 °C, with a value at room temperature approaching 10^{-3} S cm^{-1}, all suitable values for battery application.[40,42,43] The chronoamperometry and Nyquist plots recorded before and after polarization of a Li|TEGDME_LE|Li symmetrical cell in Figure 1b allow the evaluation of the Li^+-transference number (t^+) through the Bruce–Vincent–Evans method [Eq. (2) in the Experimental Section].[44] The result reported in Table 2 indicates a t^+ of 0.49, which can ensure a fast charge transfer at the electrode/electrolyte interphase of the cell.[44,45] The CV and LSV performed on Li|TEGDME_LE|SPC cells (see the Experimental Section for details) reported in Figure 1c show a sharp peak centered at 1.5 V vs. Li^+/Li related to the reduction of $LiNO_3$ and a wave around 0.8 V vs. Li^+/Li ascribed to the reductive decomposition of the TEGDME with formation of a SEI layer, as fully described in literature.[46,47] The tests also reveal a reversible processe between 0.1 and 0 V vs. Li^+/Li associated with the Li-(de)-insertion into the SPC, as well as a relevant increase of the oxidative current due to the decomposition of the solution at about 4.2 V vs. Li^+/Li, thus suggesting an electrochemical stability window of TEGDME_LE extending from 0 to 4.2 V vs. Li^+/Li.[40] The Li stripping/deposition test performed on a Li|TEGDME_LE|Li symmetrical cell in Figure 1d suggests a low overvoltage, with steady state value of 0.02 V after 500 h,

Table 2. Parameters used in Equation (2) according to Bruce–Vincent–Evans method[44] to calculate the PEGDME_LE Li^+ transference number (t^+). Specifically: the current values detected at the beginning of polarization of the Li|Li cell (i_0) and at the steady state upon measurement (i_{ss}); the resistance values achieved by NLLS fitting[49,50] of EIS performed before polarization (R_0) and at the steady state upon measurement (R_{ss}). See Figure 1 for chronoamperometric curve and Nyquist plots. See the Experimental Section for acronyms and further details.

Electrolyte	i_0 [A]	i_{ss} [A]	R_0 [Ω]	R_{ss} [Ω]	t^+
TEGDME_LE	2.98×10^{-4}	2.43×10^{-4}	71.8	64.1	0.49

© 2023 The Authors. Chemistry - A European Journal published by Wiley-VCH GmbH

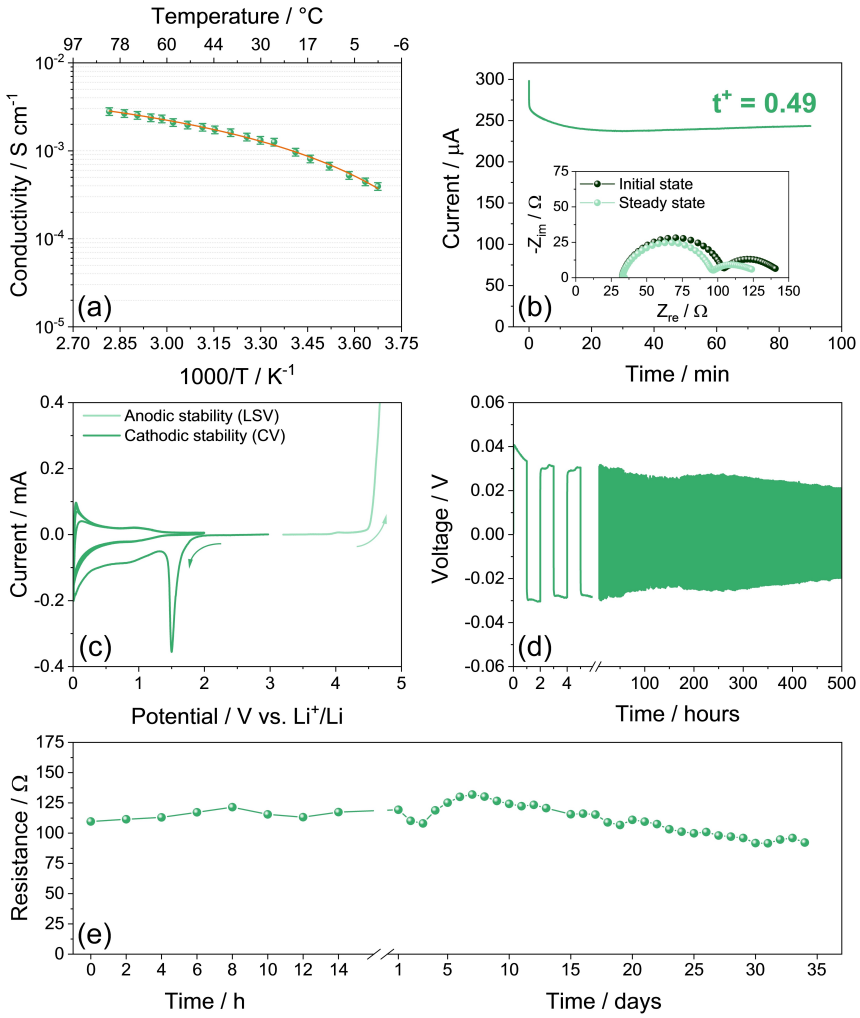

Figure 1. Electrochemical characterization of TEGDME_LE. a) Ionic conductivity plot (see corresponding Nyquist plots in Figure S1). b) Chronoamperometry curve recorded on a Li|Li symmetrical cell and related Nyquist plots acquired before and after polarization (inset) used to evaluate the electrolyte Li^+-transference number by the Bruce–Vincent–Evans method [Eq. (2) and Table 2];[44] EIS frequency range: 500 kHz–100 mHz; alternate voltage signal: 10 mV. c) Electrochemical stability window determined either by CV between 0.01 and 2.0 V vs. Li^+/Li and by LSV from cell OCV potential to 5 V vs. Li^+/Li carried out on Li|SPC cells (see the Experimental Section for details on assembly); scan rate: 0.1 mV s^{-1}. d) Li stripping/deposition test performed on a Li|Li symmetrical cell using a constant current rate of 0.1 mA cm^{-2}. e) Resistance trend vs. time achieved by regularly measuring EIS during aging of a Li|Li symmetrical cell over the 500 kHz–100 mHz frequency range by applying an alternate voltage signal of 10 mV (see corresponding Nyquist plots in Figure S2 and Table S1 for NLLS analyses).[49,50] See the Experimental Section for acronyms.

achieved upon gradual decrease of the polarization (overvoltage) due to partial dissolution and stabilization of the passivation layer at the electrode/electrolyte interphase.[48] Figure 1e shows the resistance trend of the Li/TEGDME_LE interphase determined by EIS during aging for 35 days of a cell with symmetrical configuration without any current flow. The above resistances are achieved from the corresponding Nyquist plots in Figure S2 analyzed by NLLS fits (results in Table S1). The curves are evaluated with equivalent circuits including the electrolyte resistance as high-frequency intercept of the plot with the real axis (R_e) in series with resistances and constant phase elements accounting for the electrode/electrolyte interphase semicircle at medium-high frequency (R_iQ_i), and the Warburg-type finite-length diffusion at low frequency (R_wQ_w).[49,50] The trend indicates interphase resistance values seldom exceeding 125 Ω and decreasing to 92 Ω after 35 days due to the above mentioned partial dissolution of the SEI,[14] thus suggesting a relevant chemical stability of the TEGDME_LE and its adequateness for application in Li-metal battery.[51,52]

Subsequently, the TEGDME_LE is tested in various Li cells differing by the cathode chemistry as reported in Figure 2 in order to verify its suitability. The voltage profiles of the Li|TEGDME_LE|LFP cell cycled at C/5 (1C = 170 mA g_{LFP}^{-1}) between 2.7 and 3.9 V in Figure 2a reveal the typical flat, two-phase profile related with lithium (de)insertion into the $LiFePO_4$ olivine, centered at about 3.5 V and evolving with a remarkable reversibility and very low overvoltage.[53,54] The cell delivers a capacity of 155 mA h g_{LFP}^{-1}, which is nearly the 94% of the theoretical value of the used material,[16] and retains almost 99% of the initial capacity with efficiency approaching 100% over the whole cycling test as reported in the trend of Figure 2b. This relevant performance is in line with the results

© 2023 The Authors. Chemistry - A European Journal published by Wiley-VCH GmbH

15213765, 2023, 45, Downloaded from https://chemistry-europe.onlinelibrary.wiley.com/doi/10.1002/chem.202301345 by Universita Di Ferrara, Wiley Online Library on [08/10/2024]. See the Terms and Conditions (https://onlinelibrary.wiley.com/terms-and-conditions) on Wiley Online Library for rules of use; OA articles are governed by the applicable Creative Commons License

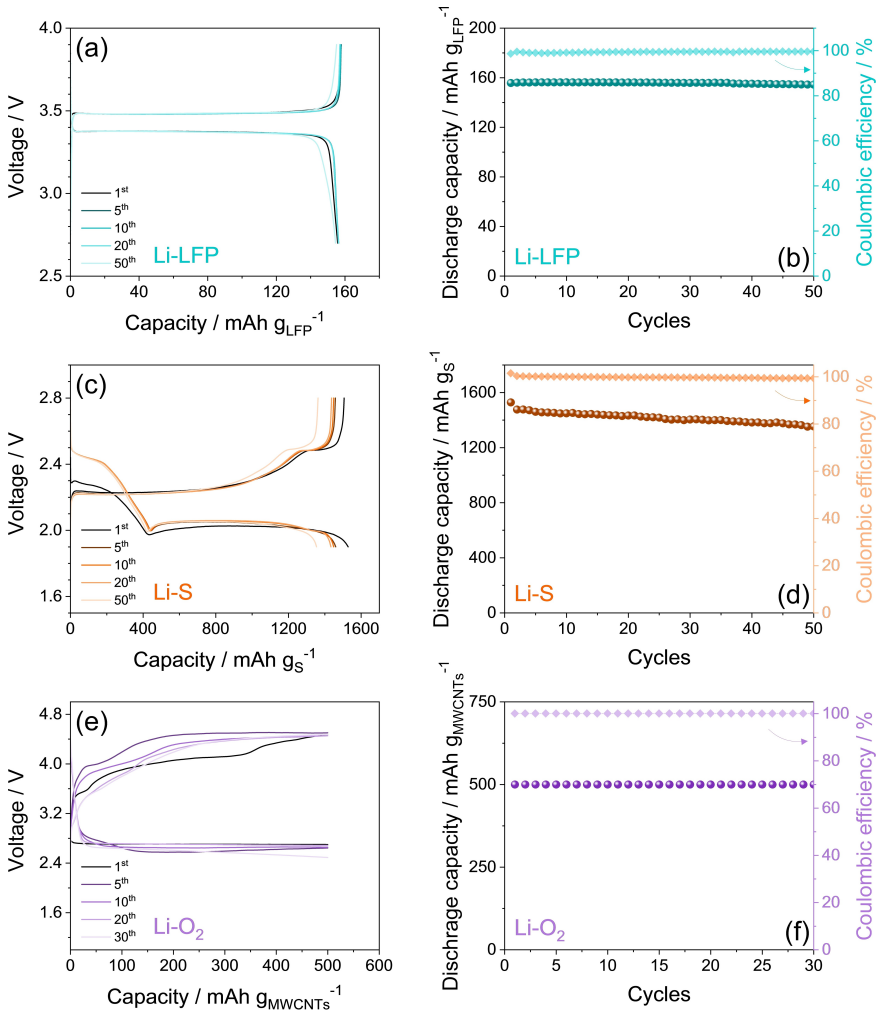

Figure 2. a), c), e) Voltage profiles and b), d), f) corresponding cycling trends (coulombic efficiency is reported on right *y*-axes) of lithium cells using TEGDME_LE and various cathode chemistries, in detail: a), b) a Li-LFP cell cycled at the constant current rate of C/5 (1C = 170 mA g_{LFP}^{-1}) between 2.7 and 3.9 V; c), d) a Li-S cell using the S@SPC-73 cathode cycled at C/10 (1C = 1675 mA g_S^{-1}) between 1.9 and 2.8 V (E/S ratio: 15 µL mg_S^{-1}); e), f) a Li-O_2 cell using the N_2@MWCNTs cathode cycled at the constant current of 100 mA g_{MWCNTs}^{-1} (MWCNTs loading: ~0.9 mg cm^{-2}) between 1.5 and 4.8 V by setting a step time of 5 h for both discharge and charge processes to limit the capacity to 500 mA h g_{MWCNTs}^{-1}. See the Experimental Section for acronyms and cell assembly details.

reported in the literature for similar electrolytes using the liquid glyme, and confirms the remarkable potentiality of TEGDME_LE for Li-metal battery application.[40] Furthermore, the Li|TEGDME_LE|S@SPC-73 cell cycled at C/10 (1C = 1675 mA g_S^{-1}) between 1.9 and 2.8 V reported in Figure 2c shows a voltage profile fully consistent with the Li-S system.[55] Indeed, the figure displays the evolution of a double plateau at 2.4 and 2.1 V leading to a capacity of the order of 1400 mA h g_S^{-1} due to the reversible conversion reaction $16Li + S_8 \leftrightarrows 8Li_2S$, which involves the formation of various soluble polysulfides having chemical formula Li_2S_x with $2 \leq x \leq 8$.[39,55–57] The above reaction appears stable over the cycles taken into account, with a retention approaching 90% and an efficiency exceeding 98% at the steady state (trend in Figure 2d). The performance in terms of voltage profiles of the Li-O_2 cell using the TEGDME_LE cycled at 100 mA g_{MWCNTs}^{-1} is reported in Figure 2e. The test is carried out by limiting the charge and discharge time to 5 h, which is reflected into a constant specific capacity of 500 mA h g^{-1} with respect to the MWCNTs mass on the GDL support. Furthermore, the cycling procedure foresees an additional voltage cutoff at 1.5 V during discharge and 4.8 V during charge. This setup is usually implemented for Li-O_2 cells in order to limit the formation of the insulating Li_2O_2 during the ORR at about 2.7 V, and mitigate the increase of the cell resistance and polarization.[58] Figure 2e shows an OER evolving below 4.7 V, while the corresponding cycling trend in Figure 2f evidences a constant capacity of 500 mA h g_{MWCNTs}^{-1} delivered over 30 cycles with an efficiency of 100%.[59,60] Hence, all the tests reported in Figure 2 suggest the TEGDME_LE as adequate media for several configuration of rechargeable energy storage systems using the lithium metal, differing by the cathode chemistry and the electrochemical responses.[42,61]

The TEGDME_LE is hereafter used to plasticize a solid polymer membrane based on crystalline PEGDME including the same salts and SiO_2 ceramic filler (PEGDME_CPE) developed previously,[14] to achieve the self-standing polymer electrolyte

© 2023 The Authors. Chemistry - A European Journal published by Wiley-VCH GmbH

15213765, 2023, 45, Downloaded from https://chemistry-europe.onlinelibrary.wiley.com/doi/10.1002/chem.202301345 by Universita Di Ferrara, Wiley Online Library on [08/10/2024]. See the Terms and Conditions (https://onlinelibrary.wiley.com/terms-and-conditions) on Wiley Online Library for rules of use; OA articles are governed by the applicable Creative Commons License

(PEGDME_PCPE) characterized in Figure 3. The photograph of Figure 3a remarks the solid nature of PEGDME_PCPE after complete vacuum removal of the TEGDME_LE (see the Experimental Section), and the slight transparency of the membrane suggests the plasticized nature which allows its direct use without further treatment in Li-metal cell operating at room temperature. The TGA and corresponding DTG in Figure 3b show for PEGDME_PCPE a thermal behavior accounting for the removal by evaporation of both TEGDME fraction below 290 °C (green line) and PEGDME around 400 °C (blue line).[27] The complexity of the DTG profiles observed between 200 and 400 °C reflects weight losses ascribed to solvated salts, solvent-salt and solvent-ceramic complexes,[62–64] whiles the peaks at temperature exceeding 400 °C are associated with the LiTFSI salt decomposition.[65] In addition, the higher residual weight observed at 800 °C for PEGDME_PCPE compared to TEGDME_LE is due to the presence of the SiO_2 ceramic filler in the former.[66] Overall, the TGA suggests relevant thermal stability of the PEGDME_PCPE, extended over 200 °C which is a key requirement for allowing sufficient safety level, in particular for electrolytes designed for the use in lithium-metal batteries.[67] A further investigation of the electrolyte features is given by the FTIR spectra reported in Figure 3c for TEGDME_LE (green line), PEGDME_CPE (orange line), and PEGDME_PCPE (blue line). In order to verify the salt dissolution in the polymer electrolyte, which is one of the most important features for allowing ion conduction, the characteristic FTIR bands expected for pure LiTFSI, that is, at 749, 773 and 810 cm^{-1} related to symmetric S–N–S stretching, at 1200 cm^{-1} due to SO_2 asymmetric stretching, and at 1320 and 1350 cm^{-1} for CF_3 asymmetric stretching,[68] are reported as dashed lines in Figure 3c. The spectra clearly demonstrate for the liquid solution (green line), the composite polymer (orange line) and for the plasticized polymer (blue line) that the LiTFSI dissociates, as indicated by the shifts in the vibrational wavenumbers of the $TFSI^-$ anion from 810, 773, and 749 cm^{-1} to lower values.[69] Furthermore, the increase of the relative peak intensities at 1350 and 1320 cm^{-1} compared to the one expected for pure LiTFSI, and the shift of the signal at 1200 cm^{-1} to lower wavenumbers, are fully consistent with a completely dissociated LiTFSI in the PEGDME_PCPE.[70] On the other hand, the similarity between the FTIR spectra of the PEGDME_PCPE and the TEGDME_LE suggests the conductive nature of the former, and its possible use as an electrolyte membrane in a lithium-metal battery.

The PEGDME_PCPE is studied in Figure 4 in terms of ionic conductivity, Li^+-transference number, electrochemical stability window, overvoltage and chemical stability in lithium cell. Analogously to TEGDME_LE, also PEGDME_PCPE reveals a conductivity trend over the temperature (Figure 4a) according to the VTF model (see corresponding Nyquist plots in Figure S3). The comparison of the data achieved by plotting the conductivity trends using Equation (1) for PEGDME_PCPE (Table 3) and TEGDME_LE (Table 1) gives raise to similar conductivity at infinite temperature (σ_∞) around 10^{-2} S cm^{-1}, which is in line with the same nature of PEGDME and TEGDME used as the solvent for the two electrolytes. The values of T_0 obtained for PEGDME_PCPE (204.1 K) and TEGDME_LE (221.2 K) allow the estimation of the glass transition point (T_g) of the two media, that is, 234 K for the liquid electrolyte and 251 K for the solid one.[71,72] It is worth mentioning that the T_g for PEGDME_PCPE is in line with that characteristic of the solid PEGDME material, thus further accounting for the mainly polymeric nature of the plasticized

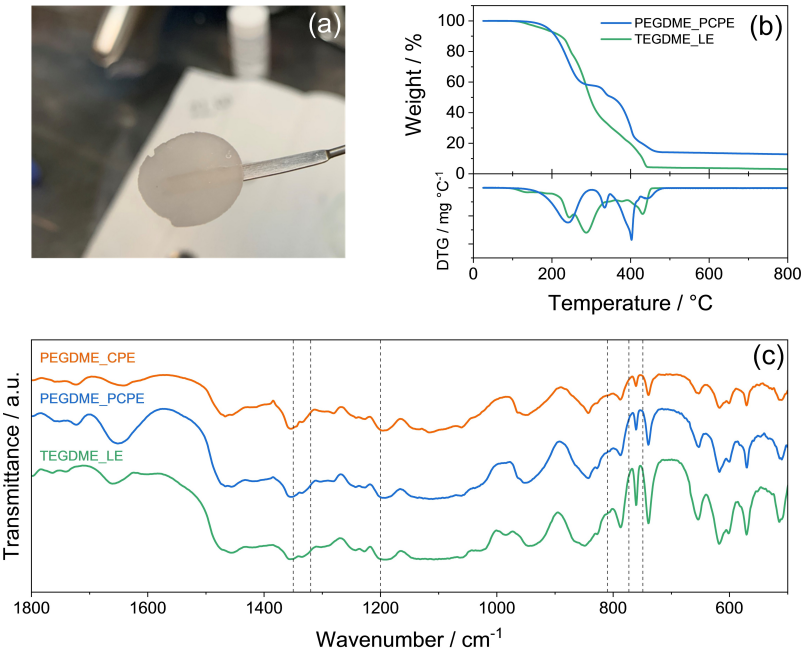

Figure 3. a) Photograph of a PEGDME_PCPE membrane with diameter of 18 mm. b) TGA (top) and corresponding DTG (bottom) of TEGDME_LE and PEGDME_PCPE recorded in the 25–800 °C temperature range at a heating rate of 5 °C min^{-1} under N_2 flow. c) FTIR spectra of TEGDME_LE, PEGDME_CPE, and PEGDME_PCPE. See the Experimental Section for acronyms.

© 2023 The Authors. Chemistry - A European Journal published by Wiley-VCH GmbH

15213765, 2023, 45, Downloaded from https://chemistry-europe.onlinelibrary.wiley.com/doi/10.1002/chem.202301345 by Universita Di Ferrara, Wiley Online Library on [08/10/2024]. See the Terms and Conditions (https://onlinelibrary.wiley.com/terms-and-conditions) on Wiley Online Library for rules of use; OA articles are governed by the applicable Creative Commons License

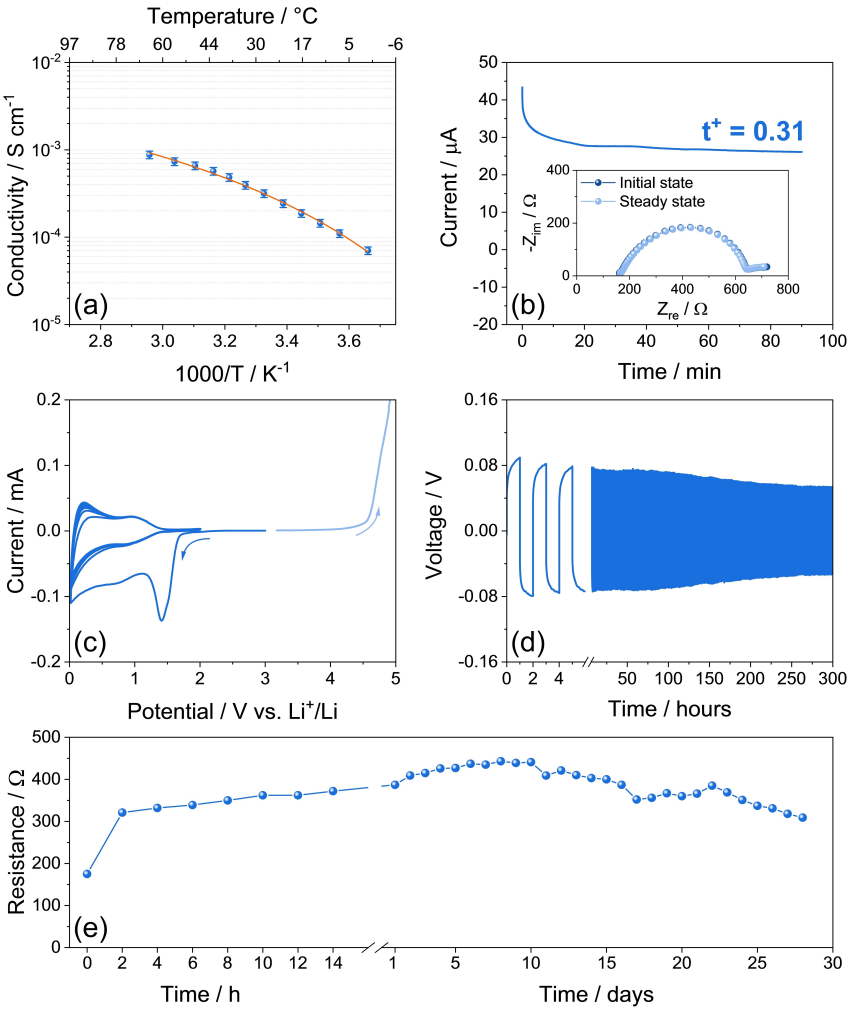

Figure 4. Electrochemical characterization of PEGDME_PCPE. a) Ionic conductivity plot (see corresponding Nyquist plots in Figure S3). b) Chronoamperometry curve recorded on a Li|Li symmetrical cell and related Nyquist plots acquired before and after polarization (inset) used to evaluate the electrolyte Li^+-transference number by the Bruce–Vincent–Evans method [Eq. (2) and Table 4];[44] EIS frequency range: 500 kHz–100 mHz; alternate voltage signal: 10 mV: c) Electrochemical stability window determined either by CV between 0.01 and 2.0 V vs. Li^+/Li and by LSV from cell OCV potential to 5 V vs. Li^+/Li carried out on Li|SPC cells (see the Experimental Section for details on assembly); scan rate: 0.1 mV s^{-1}. d) Li stripping/deposition test performed on a Li|Li symmetrical cell using a constant current rate of 0.1 mA cm^{-2}. e) Resistance trend vs. time achieved by regularly measuring EIS during aging of a Li|Li symmetrical cell in the 500 kHz–100 mHz frequency range by applying an alternate voltage signal of 10 mV (see corresponding Nyquist plots in Figure S4 and Table S2 for NLLS analyses.[49,50] See the Experimental Section for acronyms.

Table 3. Ionic conductivity at infinite temperature (σ_∞), activation energy for ion conduction (E_a), and temperature of zero configurational entropy (T_0) for the PEGDME_PCPE according to VTF equation (1) used for the conductivity trend of Figure 4a. See the Experimental Section for acronyms and further details.

Electrolyte	σ_∞ [S cm^{-1}]	E_a [eV]	T_0 [K]
PEGDME_PCPE	$14.9\times10^{-3}\pm0.1\times10^{-3}$	$32.1\times10^{-3}\pm6.3\times10^{-3}$	204.1 ± 7.1

membrane.[73] Furthermore, the data indicate a higher activation energy for Li^+ ions motion (E_a) in the polymer membrane (32.1 eV) with respect to the liquid solution (14.3 eV), as indeed expected by the higher viscosity and different transport mechanism in the former electrolyte compared to the latter one.[74–77] This difference is reflected in the value of the Li^+-transference number calculated in Figure 4b using chronoamperometry and EIS in Li|PEGDME_PCPE|Li cell. Indeed, the related data reported in Table 4 allow the determination from Equation (2) of a t^+ of 0.31 for PEGDME_PCPE, which is lower than that of TEGDME_LE (compare with Figure 1b and Table 2), but still sufficient for battery application.[78] The transference number of PEGDME_PCPE is lower than the one of TEGDME_LE due to its solid frame which may hinder the lithium ion transport and diffusion more relevantly than the liquid. Hence, the electrolyte maintains its solid nature despite the partial inclusion of TEGDME_LE in the polymer structure as a plasticizer, thus allowing higher safety level but lower performances compared to the liquid.[78] The electrochemical stability window of the polymer electrolyte is determined by CV and LSV on Li|PEGDME_PCPE|SPC cells in Figure 4c. The figure evidences the same peaks revealed for TEGDME_LE (compare with Figure 1c) accounting for the reduction of $LiNO_3$, formation of the SEI,[46,47] and Li-(de)insertion in SPC during cathodic scan with remarkable

© 2023 The Authors. Chemistry - A European Journal published by Wiley-VCH GmbH

15213765, 2023, 45, Downloaded from https://chemistry-europe.onlinelibrary.wiley.com/doi/10.1002/chem.202301345 by Universita Di Ferrara, Wiley Online Library on [08/10/2024]. See the Terms and Conditions (https://onlinelibrary.wiley.com/terms-and-conditions) on Wiley Online Library for rules of use; OA articles are governed by the applicable Creative Commons License

Table 4. Parameters used in Equation (2) according to Bruce–Vincent–Evans method[44] to calculate the PEGDME_PCPE Li^+-transference number (t^+). Specifically: the current values detected at the beginning of polarization of the Li|Li cell (i_0) and at the steady state upon measurement (i_{ss}); resistance values achieved by NLLS fitting[49,50] of EIS performed before polarization (R_0) and at the steady state upon measurement (R_{ss}). See Figure 4 for chronoamperometric curve and Nyquist plots. See the Experimental Section for acronyms and further details.

Electrolyte	i_0 [A]	i_{ss} [A]	R_0 [Ω]	R_{ss} [Ω]	t^+
PEGDME_PCPE	4.34×10^{-5}	$2.61\times10^{--5}$	486	478	0.31

stability and reversibility of the latter processe as suggested by the overlapping profiles.[79] Moreover, the figure shows the electrolyte decomposition by oxidation during the anodic sweep, which occurs at a higher potential in the polymer electrolyte with respect to the liquid one, that is, at about 4.5 V vs. Li^+/Li.[14,39] The Li stripping/deposition test in Figure 4d performed in Li|PEGDME_PCPE|Li cell reveals a low overpotential limited to 0.08 V at room temperature that decreases to 0.05 V at the end of the test due to partial SEI dissolution,[48] which is a key characteristic for allowing the proper LMB operation. Figure 4e shows the trend of the resistance over the aging time of the symmetrical cell achieved by EIS (see corresponding Nyquist plots in Figure S4, Table S2 for NLLS analyses). The data reveal an initial resistance value of about 150 Ω, progressively increasing to ~350 Ω in 14 h and to ~400 Ω in 10 days as the SEI is formed and consolidated, and then decreasing to about 310 Ω due to SEI partial dissolution.[14] It is worth mentioning that PEGDME_PCPE is characterized by higher steady state resistance compared to TEGDME_LE, that is, of about 310 Ω rather than 100 Ω, respectively. The higher electrode/electrolyte resistance of PEGDME_PCPE compared to TEGDME_LE is in line with the higher E_a and the lower t^+ in the former compared to the latter, which in turn hinder the kinetics of the charge transfer process.[12] Furthermore, Figure 4e indicates that the resistance value remains stable, with minor fluctuations over one month of aging, thus suggesting the formation of a favorable SEI at the electrode/electrolyte interphase which can promote the use of PEGDME_PCPE in LMB.[39]

The polymer electrolyte is used in Figure 5 in Li|PEGDME_PCPE|LFP cell cycled at C/10 (1C = 170 mA g_{LFP}^{-1}) between 2.7 and 3.9 V (Figure 5a, b), Li|PEGDME_PCPE|S@SPC-73 cell cycled at C/20 (1C = 1675 mA g_S^{-1}) between 1.6 and 2.8 V for one activation cycle and in the 1.7–2.8 V range during subsequent ones (Figure 5c, d), and Li|PEGDME_PCPE|O_2 cell cycled at the constant current of 100 mA g_{MWCNTs}^{-1} by setting a charge/discharge time of 5 h to limit the capacity at 500 mA h g_{MWCNTs}^{-1} between 1.5 and 4.8 V (Figure 5e, f). The voltage signature of the Li|PEGDME_PCPE|LFP cell in Figure 5a reveals an initial cycle with a higher charge polarization, and lower discharge capacity compared to the analogue cell using the liquid electrolyte (compare with Figure 2a). Subsequently, the polarization of the cell using PEGDME_PCPE decreases and the capacity increases, to reach similar values compared the cell using TEGDME_LE, that is, a capacity of about 150 mA h g^{-1} and a polarization below 0.15 V in line with an efficient Li-(de)insertion process into the $LiFePO_4$ olivine.[16] The improvement of the cell is even more evident in Figure 5b which reports the cycling trend, and shows a capacity progressively increasing from about 115 mA h g_{LFP}^{-1} at the initial cycle to about 150 mA h g_{LFP}^{-1}, and an efficiency approaching 100% at the steady state. This behavior, already observed in lithium cells using analogue PEO-based electrolytes and LFP cast including PVDF binder, is typically ascribed to the increase of the electrode/electrolyte interphase ionic conductivity upon the progressive wetting of the electrode during operation, and to the formation of a favorable blend between the polymer electrolyte and the binder allowing a faster motion of the Li^+ ions compared to the pristine state.[9,12,80] The voltage profile of the Li|PEGDME_PCPE|S@SPC-73 cell reported in Figure 5c depicts during the first cycle a similar signature to the one with the liquid electrolyte (compare with Figure 2c), reflecting the reversible conversion reaction between Li and S, although a lower capacity of about 1200 mA h g_S^{-1} and higher polarization are observed. This difference may account for the above mentioned slower kinetics of the charge transfer for the Li-S cell using the polymer electrolyte compared to the liquid one, despite a lower discharge cutoff (1.7 V rather than 1.9 V) and cycling rate (C/20 instead of C/10) are used in the former compared to the latter. It is worth mentioning that the first discharge in the polymer cell is performed at a lower cutoff with respect to the following cycles, that is, 1.6 V, in order to allow the consolidation of adequate SEI at the electrode/electrolyte interphase.[39,55,56] The voltage profiles of Figure 5c evolve with a capacity progressively decreasing, in line with the increase of the cell resistance from ~200 to about 400 Ω already observed in the first stages in Figure 4e, and subsequently stabilizing at ~400 mA h g_S^{-1}. The corresponding cycling trend in Figure 5d is characterized by an efficiency approaching 100% at the end of the test, and accounts for the formation of a suitable electrode/electrolyte interphase in the polymer Li-S cell. It is worth mentioning that the decrease of the Li-S cell capacity may be ascribed to a partial loss of the active material dissolved in the polymer matrix due to the limited diffusion of the Li_2S_x species, which in turns can contribute to the formation of a suitable interphase and allow safe cycling without polysulfides shuttle.[27] On the other hand, the voltage profiles of the polymer Li|PEGDME_PCPE|O_2 cell reported in Figure 5e shows relevant differences compared to the liquid cell of Figure 2e. The first discharge process reflecting the ORR occurs at a lower voltage using PEGDME_PCPE (2.5 V) compared to TEGDME_LE (2.7 V), thus suggesting a higher polarization. Furthermore, the first discharge delivers 500 mA h g_{MWCNTs}^{-1} which is the capacity expected by the adopted time limit, while the subsequent charge (OER) appears incomplete and leads to a capacity of about 180 mA h g_{MWCNTs}^{-1} with very low efficiency (~35%) considered in this case as charge/discharge ratio for better visualization, as also evidenced in the corresponding trend of Figure 5f. After the first cycle, the charge capacity progressively increases, and the efficiency improves to values approaching 90% at the 14th cycle. This behavior reflects a slower kinetics of the OER in the polymer Li-O_2 cell compared to the liquid one, and suggests the need for further tuning of the electrode/electrolyte interphase to increase the wettability, and the use of a catalyst to fasten the reaction in the three-phases (solid/polymer/gas) system.[81–84] Nevertheless, the stable discharge capacity trend observed in Figure 5f represents a promising

© 2023 The Authors. Chemistry - A European Journal published by Wiley-VCH GmbH

15213765, 2023, 45, Downloaded from https://chemistry-europe.onlinelibrary.wiley.com/doi/10.1002/chem.202301345 by Universita Di Ferrara, Wiley Online Library on [08/10/2024]. See the Terms and Conditions (https://onlinelibrary.wiley.com/terms-and-conditions) on Wiley Online Library for rules of use; OA articles are governed by the applicable Creative Commons License

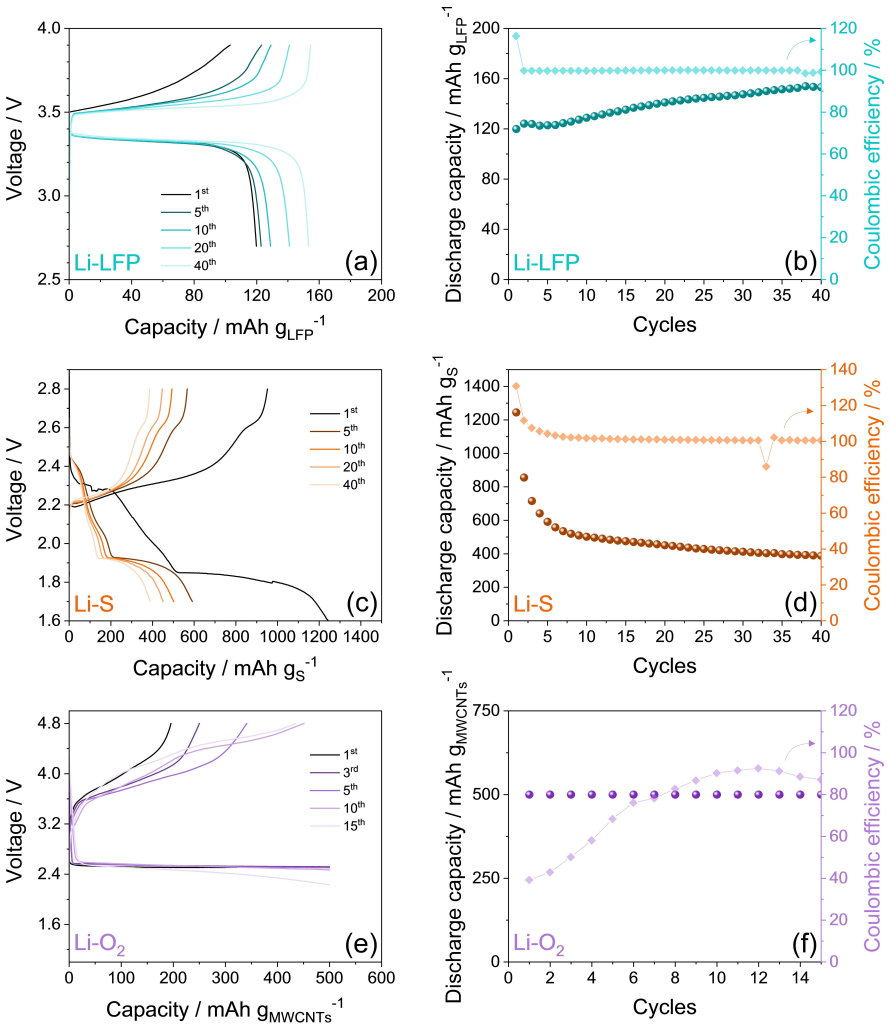

Figure 5. a), c), e) Voltage profiles and b), d), f) corresponding cycling trends (coulombic efficiency is reported on right *y*-axes) of lithium cells using PEGDME_PCPE and various cathode chemistries, in detail: a), b) a Li-LFP cell cycled at the constant current rate of C/10 (1C = 170 mA g_{LFP}^{-1}) between 2.7 and 3.9 V; c), d) a Li-S cell using the S@SPC-73 cathode cycled at C/10 (1C = 1675 mA g_S^{-1}) between 1.7 and 2.8 V after one activation cycle at C/20 in the 1.6–2.8 V voltage range; e), f) a Li-O_2 cell using the N_2@MWCNTs cathode cycled at the constant current of 100 mA g_{MWCNTs}^{-1} (MWCNTs loading: ~0.9 mg cm^{-2}) between 1.5 and 4.8 V by setting a step time of 5 h for both discharge and charge processes to limit the capacity to 500 mA h g_{MWCNTs}^{-1}. See the Experimental Section for acronyms and cell assembly details.

preliminary result for the development of a safe and high capacity Li-O_2 polymer cell.[85]

Conclusions

A polymer electrolyte based on solid PEGDME plasticized by a TEGDME solution has been developed and studied in lithium metal batteries operating at room temperature with $LiFePO_4$, sulfur, and oxygen cathodes. The electrolyte revealed thermal stability extending over 200 °C, and a solid structure in which the SiO_2 ceramic is well dispersed and lithium salts are efficiently dissolved. The polymer electrolyte showed a room temperature conductivity exceeding 10^{-4} S cm^{-1}, a Li^+-transference number of 0.31, electrochemical stability ranging from 0 to 4.4 V vs. Li^+/Li, a Li-stripping deposition overvoltage lower than 0.08 V, and stable electrode/electrolyte interphase with resistance lower than 400 Ω. FTIR spectra demonstrated the complete dissociation of the LiTFSI salt in PEGDME_PCPE by the shift of the vibrational wavenumbers 749, 773 and 810 cm^{-1} related with symmetric S–N–S stretching of the $TFSI^-$ to lower values, an increase in the relative peak intensities at 1350 and 1320 cm^{-1} of CF_3 asymmetric stretching, and a shift in the signal at 1200 cm^{-1} due to SO_2 groups asymmetric stretching of $TFSI^-$ to lower wavenumbers. The Li-$LiFePO_4$ polymer cell revealed initial high polarization, which subsequently decreased to reach a steady state capacity of ~150 mA h g_{LFP}^{-1} and polarization below 0.15 V, thus suggesting efficient Li-(de)insertion process into the olivine cathode. This behavior has been ascribed to an increase in the electrode/electrolyte interphase ionic conductivity through progressive wetting of the electrode, and the formation of a suitable blend between polymer electrolyte and electrode binder allowing fast Li^+ motion. The Li-S cell revealed a reversible conversion reaction between Li and S according to the overall electrochemical process $16Li + S_8 \leftrightarrows 8Li_2S$, with an initial discharge capacity of

© 2023 The Authors. Chemistry - A European Journal published by Wiley-VCH GmbH

15213765, 2023, 45, Downloaded from https://chemistry-europe.onlinelibrary.wiley.com/doi/10.1002/chem.202301345 by Universita Di Ferrara, Wiley Online Library on [08/10/2024]. See the Terms and Conditions (https://onlinelibrary.wiley.com/terms-and-conditions) on Wiley Online Library for rules of use; OA articles are governed by the applicable Creative Commons License

1200 mA h g_S^{-1}, decreasing and stabilizing during the subsequent cycles to about 400 mA h g_S^{-1}. The Li-O_2 polymer cell showed a first discharge process accounting for an ORR at 2.5 V with a capacity of 500 mA h g_{MWCNTs}^{-1}, and incomplete subsequent charge (OER) with a capacity of 180 mA h g_{MWCNTs}^{-1} and low efficiency (~35%). After the first cycle, the charge capacity progressively increased, and the efficiency improved to values approaching 90%. This behavior was attributed to kinetics and wettability limits during ORR and OER processes, evolving in a complex solid/polymer/gas interphase that might require the use of catalysts to improve the reaction kinetics. The promising results achieved in this work, in addition to the relevant safety content of the cells, suggest the polymer electrolyte studied herein as a suitable medium for safe room temperature LMBs exploiting a vast range of cathodes and differing by energy content and characteristic electrochemical process.

Experimental Section

Electrolytes preparation: The liquid electrolyte (LE) plasticizing agent was prepared in an Ar-filled glovebox (MBraun, H_2O and O_2 levels under 1 ppm) by dissoving lithium bis(trifluoromethanesulfonyl)-imide (LiTFSI, $LiN(SO_2)_2(CF_3)_2$, 99.95% trace metal basis, Sigma-Aldrich) conductive salt and lithium nitrate ($LiNO_3$, 99.99% trace metal basis, Sigma-Aldrich) additive in tetra(ethylene glycol)dimethyl ether (TEGDME, $CH_3(OCH_2CH_2)_4OCH_3$, ≥99%, Sigma-Aldrich) with a concentration of 1 mol $kg_{solvent}^{-1}$ for each salt. Before using, LiTFSI and $LiNO_3$ were dried under vacuum at 110 °C for 2 days, while TEGDME was stored under dry molecular sieves (rods, 3 Å, size 1/16 in., Honeywell Fluka) to achieve a water content lower than 10 ppm as verified by a Karl Fischer 899 Coulometer (Metrohm). The TEGDME-solution is indicated in the text as TEGDME_LE.

The composite polymer electrolyte (CPE) precursor was prepared according with a previous paper.[14] Poly(ethylene glycol)dimethyl ether powder (PEGDME, $CH_3(OCH_2CH_2)_nOCH_3$, average molecular weight 2000 g mol^{-1}, Sigma-Aldrich) was initially mixed with LiTFSI and $LiNO_3$ to achieve a concentration of 1 mol kg_{PEGDME}^{-1} for each salt, afterwards, fumed silica powder (SiO_2, average particle size: 0.007 μm, Sigma-Aldrich) was added to the polymer-salts mixture by a 10% weight ratio. The components were dispersed/dissolved in acetonitrile (ACN, CH_3CN, Sigma-Aldrich) and magnetically stirred for two days to obtain a viscous slurry, which was cast on a plastic foil (23-5FEP-2-50, CS Hyde) by doctor blade (MTI Corporation) technique. Upon several drying steps performed under vacuum,[14] the membrane was introduced in an Ar-filled glovebox and stored at 25 °C for about 20 days to achieve complete solidification. Subsequently, the polymer electrolyte was cut into membranes with diameter of either 10 or 18 mm, which were soaked for two days with an excess of TEGDME_LE to allow uniform wetting, and subsequently dried under vacuum for 5 h to remove the liquid excess and obtain a new plasticized composite polymer electrolyte (PCPE) indicated in the text as PEGDME_PCPE.

Electrolytes characterization: TGA of TEGDME_LE and PEGDME_PCPE were carried out by a Mettler-Toledo TGA 2 instrument in the 25–800 °C temperature range using a heating rate of 5 °C min^{-1} under a N_2 flow of 50 mL min^{-1}.

FTIR spectra of TEGDME_LE, PEGDME_CPE and PEGDME_PCPE were acquired using a Bruker Vertex V70 instrument set up in the transmittance mode.

The electrochemical properties of TEGDME_LE and PEGDME_PCPE were evaluated in CR2032 coin-type cells (MTI Corporation) with various configuration assembled in an Ar-filled glovebox. The ionic conductivity was investigated by performing EIS at various temperatures in the 500 kHz–100 Hz frequency range through an alternate voltage signal of 10 mV on blocking-electrode stainless-steel | electrolyte | stainless-steel symmetrical cells using either one O-ring (23-5FEP-2–50, CS Hyde, internal diameter of 10 mm) filled with TEGDME_LE, or two O-rings holding a 10 mm-diameter PEGDME_PCPE membrane. The O-ring thickness of 127 μm allowed to fix the cell constant at 0.016 cm^{-1} for TEGDME_LE and 0.032 cm^{-1} for PEGDME_PCPE. The temperature of the cells was controlled via a F12 Julabo instrument.

The Li^+-transference number (t^+) was evaluated by applying the Bruce–Vincent–Evans method.[44] Symmetrical cells with Li | electrolyte | Li configuration were prepared by using two 14 mm-diameter lithium discs separated either by four 16 mm-diameter glass fiber Whatman® GF/A discs soaked with TEGDME_LE or by two O-rings holding a 10 mm-diameter PEGDME_PCPE membrane. A chronoamperometry test was carried out on the cells by applying a voltage (ΔV) of 30 mV for 90 min, and EIS was performed before and after polarization using the 500 kHz–100 mHz frequency range and an alternate voltage signal of 10 mV. The voltage, current, and resistance values were used in Equation (2) to calculate t^+:[44]

$$t^+ = \frac{i_{ss}}{i_0} \times \frac{(\Delta V - R_0 i_0)}{(\Delta V - R_{ss} i_{ss})} \quad (2)$$

where i_0 and i_{ss} are the current values at the initial and steady state, respectively, and R_0 and R_{ss} are the interphase resistance values before and after cell polarization, respectively, calculated from the impedance spectra (see below for fitting method).

Carbon-based electrodes were prepared by doctor blade casting on either Al or Cu foils of a slurry obtained by dispersing carbon black (80%, Super P carbon, SPC, Timcal) and polyvinilidene fluoride (20%, PVDF, Solef® 6020) polymer binder in *N*-methyl-2-pyrrolidone (NMP, Sigma-Aldrich). The slurries were dried on hot plates at 70 °C to remove the NMP solvent, cut into discs with diameter of either 14 mm or 10 mm and dried under vacuum at 110 °C for 3 h before being transferred in an Ar-filled glovebox. The electrochemical stability window of the electrolytes was determined by cyclic voltammetry (CV) measurements on Li | electrolyte | SPC-Cu cells between 0.01 and 2.0 V vs. Li^+/Li at 0.1 mV s^{-1} and by linear sweep voltammetry (LSV) on Li | electrolyte | SPC-Al cells from the open circuit voltage (OCV) to 5.0 V vs. Li^+/Li at 0.1 mV s^{-1}. The Li | SPC cells used either a 14 mm-diameter lithium disc separated from a 14 mm-diameter SPC electrode by two 16 mm-diameter glass fiber Whatman® GF/A discs soaked with TEGDME_LE, or a 14 mm lithium disc separated from a 10 mm-diameter SPC electrode by two O-rings holding a 10 mm-diameter PEGDME_PCPE membrane.

Lithium stripping/deposition tests were carried out on Li | electrolyte | Li symmetrical cells through galvanostatic cycling measurements using a constant current of 0.1 mA cm^{-2} and setting a step time of 1 h for both charge and discharge processes. The cells were assembled by stacking two 14 mm-diameter lithium discs separated either by two 16 mm-diameter glass fiber Whatman® GF/A discs soaked with TEGDME_LE or by two O-rings holding a 10 mm-diameter PEGDME_PCPE membrane.

The same cell configurations were adopted to investigate the electrolytes stability upon aging in contact with lithium metal by performing EIS measurements on Li | electrolyte | Li cells every 2 h for the first 14 h since assembly and subsequently every day for about 30 days.

All the Nyquist plots recorded by EIS were fitted through nonlinear least-squares (NLLS) method with the aid of the Boukamp software[49,50] and only fits with a χ^2 value of the order of 10^{-4} or lower were considered suitable. The fitting allowed the description of the Nyquist plots with equivalent circuits including resistive (R) and capacitive (Q) elements, in particular: i) R_e, which is the electrolyte

© 2023 The Authors. Chemistry - A European Journal published by Wiley-VCH GmbH

15213765, 2023, 45, Downloaded from https://chemistry-europe.onlinelibrary.wiley.com/doi/10.1002/chem.202301345 by Universita Di Ferrara, Wiley Online Library on [08/10/2024]. See the Terms and Conditions (https://onlinelibrary.wiley.com/terms-and-conditions) on Wiley Online Library for rules of use; OA articles are governed by the applicable Creative Commons License

resistance and is indicated by the high-frequency intercept of the plot; ii) a series of (*RQ*) elements describing either the charge transfers at the electrode/electrolyte interphase, that is, (R_iQ_i) associated to the high-medium frequency semicircle, or the finite-length Warburg-type Li^+ diffusion, namely, (R_wQ_w) identified by the low frequency semicircle.

The voltammetry and EIS tests were performed via a VersaSTAT MC Princeton Applied Research (PAR-AMETEK) instrument, while the galvanostatic cycling measurements were carried out using a MACCOR series 4000 battery test system.

Electrolytes application: The cathodes used in lithium cell employed various active materials, in detail: i) $LiFePO_4$ (LFP) with a carbon content of about 5% was developed by Advanced Lithium Electrochemistry (Aleees Taiwan, model A1100);[16] ii) a sulfur-carbon composite, which was prepared by mixing elemental sulfur (≥99.5%, Riedel-de Haën) with SPC by the 70:30 weight ratio, followed by heating at 125 °C under magnetic stirring with the aid of a silicon oil bath until complete melting of sulfur and blending with SPC, subsequent quenching at room temperature and grinding of the final composite indicated in the text as S@SPC-73;[55] iii) multiwalled carbon nanotubes (MWCNTs, > 90% carbon basis, D×L: 110–170 nm×5–9 μm, Sigma-Aldrich), which were annealed at 750 °C for 12 h under N_2 flow to achieve the N_2@MWCNTs.[58] The electrode slurries were prepared by dispersing in NMP solvent the following mixtures: i) LFP/SPC/PVDF 80:10:10 wt.%; ii) S@SPC-73/SPC/PVDF 80:10:10 wt.%; iii) N_2@MWCNTs/PVDF 80:20 wt.%. The slurries were cast via doctor blade technique on either a carbon-coated Al foil (thickness of 20 μm, MTI Corporation) for LFP, a porous carbon-cloth ELAT 1400 gas diffusion layer (GDL, MTI Corporation) for S@SPC-73, or a 39BC GDL (SiGracet) for N_2@MWCNTs. The LFP and N_2@MWCNTs electrode tapes were dried on a hot plate for 3 h at 70 °C and cut into 14 mm-diameter (LFP) and 16 mm-diameter (N_2@MWCNTs) discs which were dried for 3 h at 110 °C under vacuum before being transferred in an Ar-filled glovebox, while the S@SPC-73 tape was dried at room temperature until complete evaporation of NMP and cut into 14 mm-diameter discs which were dried at 35 °C overnight under vacuum before transfer. The final active material loadings of the cathodes were between 4.3 and 4.8 mg cm^{-2} for LFP (electrode geometric area: 1.54 cm^2), between 1.3 and 1.4 mg_S cm^{-2} for S@SPC-73 (electrode geometric area: 1.54 cm^2), and of 0.9 mg_{MWCNTs} cm^{-2} for N_2@MWCNTs (electrode geometric area: 2.01 cm^2).

The electrolytes were tested in CR2032 coin-type lithium cells using a 14 mm-diameter lithium disc as anode, one of the cathodes described above, and different electrolyte/separator combinations, in particular: Li|TEGDME_LE|cathode cells employed i) one 16 mm-diameter glass fiber Whatman® GF/B disc as separator for LFP, ii) one 16 mm-diameter Celgard 2400 separator soaked with the electrolyte by the 15 μL mg^{-1} electrolyte/sulfur (E/S) ratio for S@SPC-73, and iii) two 18 mm-diameter glass fiber Whatman® GF/A discs for N_2@MWCNTs; on the other hand, Li|PEGDME_PCPE|cathode cells employed a 18 mm-diameter PEGDME_PCPE membrane separating Li anode and cathode. Regular CR2032 coin-type cells were used for Li-LFP and Li-S cells, while top-meshed CR2032 cells (MTI Corporation) inserted in pure O_2-filled glass tubes were used to achieve the Li-O_2 cells.

Li-LFP cells were galvanostatically cycled between 2.7 and 3.9 V at either C/5 or C/10 (1C = 170 mA g_{LFP}^{-1}) whether using TEGDME_LE or PEGDME PCPE, respectively. Cycling tests were performed on Li-S cells at C/10 (1C = 1675 mA g_S^{-1}) in the 1.9–2.8 V voltage range for Li|TEGDME_LE|S@SPC-73 configuration, while one activation cycle at C/20 between 1.6 and 2.8 V followed by prolonged cycling at C/20 in the 1.7–2.8 V voltage range was employed for Li|PEGDME_PCPE|S@SPC-73 configuration. Finally, Li-O_2 cells were cycled in the 1.5–4.8 V voltage range at the constant rate of 100 mA g_{MWCNTs}^{-1} by setting a step time of 5 h for both discharge and charge to limit the cell capacity at 500 mA h g_{MWCNTs}^{-1}. The galvanostatic cycling measurements were performed through a MACCOR series 4000 battery test system setting room temperature at 30 °C with a maximum fluctuation of ±0.1 °C.

Acknowledgements

This project has been funded under the National Recovery and Resilience Plan (NRRP), Mission 04 Component 2 Investment 1.5 – NextGenerationEU, Call for tender no. 3277 dated 30/12/2021, award no. 0001052 dated 23/06/2022. The authors also thank the European Union's Horizon2020 research and innovation programme Graphene Flagship under grant agreement no. 881603, the grant "Fondo di Ateneo per la Ricerca Scientifica, FAR 2022" University of Ferrara, and the project "Accordo di Collaborazione Quadro 2015" between University of Ferrara (Department of Chemical and Pharmaceutical Sciences) and Sapienza University of Rome (Department of Chemistry).

Conflict of Interests

The authors declare no conflict of interest.

Data Availability Statement

The data that support the findings of this study are available in the supplementary material of this article.

Keywords: lithium metal batteries · $LiFePO_4$ · oxygen · solid PEGDME electrolytes · sulfur

[1] W. Xu, J. Wang, F. Ding, X. Chen, E. Nasybulin, Y. Zhang, J.-G. Zhang, *Energy Environ. Sci.* **2014**, *7*, 513.
[2] A. Varzi, K. Thanner, R. Scipioni, D. Di Lecce, J. Hassoun, S. Dörfler, H. Altheus, S. Kaskel, C. Prehal, S. A. Freunberger, *J. Power Sources* **2020**, *480*, 228803.
[3] D. Lin, Y. Liu, Y. Cui, *Nat. Nanotechnol.* **2017**, *12*, 194.
[4] Y. Wang, B. Liu, Q. Li, S. Cartmell, S. Ferrara, Z. D. Deng, J. Xiao, *J. Power Sources* **2015**, *286*, 330.
[5] M. L. Meyerson, J. K. Sheavly, A. Dolocan, M. P. Griffin, A. H. Pandit, R. Rodriguez, R. M. Stephens, D. A. Vanden Bout, A. Heller, C. B. Mullins, *J Mater Chem A Mater* **2019**, *7*, 14882.
[6] J. B. Goodenough, Y. Kim, *Chem. Mater.* **2010**, *22*, 587.
[7] D. Aurbach, E. Zinigrad, Y. Cohen, H. Teller, *Solid State Ion* **2002**, *148*, 405.
[8] C. Li, S. Zhang, X. Miao, C. Wang, C. Wang, Z. Zhang, R. Wang, L. Yin, *Batter Supercaps* **2022**, *5*, e202100288.
[9] G. B. Appetecchi, F. Croce, J. Hassoun, B. Scrosati, M. Salomon, F. Cassel, *J. Power Sources* **2003**, *114*, 105.
[10] W. Lyu, G. He, T. Liu, *ChemistryOpen* **2020**, *9*, 713.
[11] R. Lei, Y. Yang, C. Yu, Y. Xu, Y. Li, J. Li, *Sustain. Energy Fuels* **2021**, *5*, 1538.
[12] G. B. Appetecchi, J. Hassoun, B. Scrosati, F. Croce, F. Cassel, M. Salomon, *J. Power Sources* **2003**, *124*, 246.
[13] I. Gracia, M. Armand, D. Shanmukaraj in *Solid Electrolytes for Advanced Applications* Springer International, Cham, **2019**, pp. 347–373, Eds. R. Murugan, W. Weppner.
[14] V. Marangon, Y. Tominaga, J. Hassoun, *J. Power Sources* **2020**, *449*, 227508.
[15] H. Huo, M. Jiang, B. Mogwitz, J. Sann, Y. Yusim, T. Zuo, Y. Moryson, P. Minnmann, F. H. Richter, C. Veer Singh, J. Janek, *Angew. Chem. Int. Ed.* **2023**, *62*, e202218044.

© 2023 The Authors. Chemistry - A European Journal published by Wiley-VCH GmbH

15213765, 2023, 45, Downloaded from https://chemistry-europe.onlinelibrary.wiley.com/doi/10.1002/chem.202301345 by Universita Di Ferrara, Wiley Online Library on [08/10/2024]. See the Terms and Conditions (https://onlinelibrary.wiley.com/terms-and-conditions) on Wiley Online Library for rules of use; OA articles are governed by the applicable Creative Commons License

[16] S. Brutti, J. Hassoun, B. Scrosati, C.-Y. Lin, H. Wu, H.-W. Hsieh, *J. Power Sources* **2012**, *217*, 72.
[17] Y. Wang, P. He, H. Zhou, *Energy Environ. Sci.* **2011**, *4*, 805.
[18] L. Carbone, S. G. Greenbaum, J. Hassoun, *Sustain. Energy Fuels* **2017**, *1*, 228.
[19] H.-J. Peng, J.-Q. Huang, X.-B. Cheng, Q. Zhang, *Adv. Energy Mater.* **2017**, *7*, 1700260.
[20] L. Grande, E. Paillard, J. Hassoun, J.-B. Park, Y.-J. Lee, Y.-K. Sun, S. Passerini, B. Scrosati, *Adv. Mater.* **2015**, *27*, 784.
[21] S. Drvarič Talian, J. Moškon, R. Dominko, M. Gaberšček, *ACS Appl. Mater. Interfaces* **2017**, *9*, 29760.
[22] L. Zhou, D. L. Danilov, R. Eichel, P. H. L. Notten, *Adv. Energy Mater.* **2021**, *11*, 2001304.
[23] C. Li, Z. Xi, D. Guo, X. Chen, L. Yin, *Small* **2017**, *14*, 1701986.
[24] R. Black, S. H. Oh, J.-H. Lee, T. Yim, B. Adams, L. F. Nazar, *J. Am. Chem. Soc.* **2012**, *134*, 2902.
[25] J. Herranz, A. Garsuch, H. A. Gasteiger, *J. Phys. Chem. C* **2012**, *116*, 19084.
[26] P. Hartmann, D. Grübl, H. Sommer, J. Janek, W. G. Bessler, P. Adelhelm, *J. Phys. Chem. C* **2014**, *118*, 1461.
[27] V. Marangon, D. Di Lecce, L. Minnetti, J. Hassoun, *ChemElectroChem* **2021**, *8*, 3971.
[28] J. Hassoun, B. Scrosati, *Adv. Mater.* **2010**, *22*, 5198.
[29] G. Ma, F. Huang, Z. Wen, Q. Wang, X. Hong, J. Jin, X. Wu, *J Mater Chem A Mater* **2016**, *4*, 16968.
[30] S. S. Jeong, Y. T. Lim, Y. J. Choi, G. B. Cho, K. W. Kim, H. J. Ahn, K. K. Cho, *J. Power Sources* **2007**, *174*, 745.
[31] M. Agostini, J. Hassoun, *Sci. Rep.* **2015**, *5*, 7591.
[32] G. A. Elia, J. Hassoun, *Sci. Rep.* **2015**, *5*, 12307.
[33] Q. Wang, Z. Wen, J. Jin, J. Guo, X. Huang, J. Yang, C. Chen, *Chem. Commun.* **2016**, *52*, 1637.
[34] M. Liu, D. Zhou, H. R. Jiang, Y. X. Ren, F. Y. Kang, T. S. Zhao, *Nano Energy* **2016**, *28*, 97.
[35] Y. T. Kim, E. S. Smotkin, *Solid State Ion* **2002**, *149*, 29.
[36] H. Horie, T. Abe, T. Kinoshita, Y. Shimoida, *World Electric Vehicle Journal* **2008**, *2*, 25.
[37] D. Di Lecce, R. Verrelli, J. Hassoun, *Green Chem.* **2017**, *19*, 3442.
[38] P. J. Carvalho, C. H. G. Fonseca, M.-L. C. J. Moita, Â. F. S. Santos, J. A. P. Coutinho, *J. Chem. Eng. Data* **2015**, *60*, 3721.
[39] D. Di Lecce, V. Marangon, H.-G. Jung, Y. Tominaga, S. Greenbaum, J. Hassoun, *Green Chem.* **2022**, *24*, 1021.
[40] S. Wei, S. Inoue, D. Di Lecce, Z. Li, Y. Tominaga, J. Hassoun, *ChemElectroChem* **2020**, *7*, 2376.
[41] G. A. Elia, U. Ulissi, S. Jeong, S. Passerini, J. Hassoun, *Energy Environ. Sci.* **2016**, *9*, 3210.
[42] M. Nojabaee, J. Popovic, J. Maier, *J Mater Chem A Mater* **2019**, *7*, 13331.
[43] C. Pfaffenhuber, F. Hoffmann, M. Fröba, J. Popovic, J. Maier, *J Mater Chem A Mater* **2013**, *1*, 12560.
[44] J. Evans, C. A. Vincent, P. G. Bruce, *Polymer (Guildf)* **1987**, *28*, 2324.
[45] J. Popovic, D. Höfler, J. P. Melchior, A. Münchinger, B. List, J. Maier, *J. Phys. Chem. Lett.* **2018**, *9*, 5116.
[46] S. S. Zhang, *Electrochim. Acta* **2012**, *70*, 344.
[47] A. Rosenman, R. Elazari, G. Salitra, E. Markevich, D. Aurbach, A. Garsuch, *J. Electrochem. Soc.* **2015**, *162*, A470.
[48] S. Phadke, E. Coadou, M. Anouti, *J. Phys. Chem. Lett.* **2017**, *8*, 5907.
[49] B. Boukamp, *Solid State Ion* **1986**, *18–19*, 136.
[50] B. Boukamp, *Solid State Ion* **1986**, *20*, 31.
[51] K. Xu, *Chem. Rev.* **2004**, *104*, 4303.
[52] X. He, D. Bresser, S. Passerini, F. Baakes, U. Krewer, J. Lopez, C. T. Mallia, Y. Shao-Horn, I. Cekic-Laskovic, S. Wiemers-Meyer, F. A. Soto, V. Ponce, J. M. Seminario, P. B. Balbuena, H. Jia, W. Xu, Y. Xu, C. Wang, B. Horstmann, R. Amine, C.-C. Su, J. Shi, K. Amine, M. Winter, A. Latz, R. Kostecki, *Nat. Rev. Mater.* **2021**, *6*, 1036.
[53] C. A. J. Fisher, M. S. Islam, *J. Mater. Chem.* **2008**, *18*, 1209.
[54] F. Gao, Z. Tang, *Electrochim. Acta* **2008**, *53*, 5071.
[55] D. Di Lecce, V. Marangon, W. Du, D. J. L. Brett, P. R. Shearing, J. Hassoun, *J. Power Sources* **2020**, *472*, 228424.
[56] V. Marangon, C. Hernández-Rentero, M. Olivares-Marín, V. Gómez-Serrano, Á. Caballero, J. Morales, J. Hassoun, *ChemSusChem* **2021**, *14*, 3333.
[57] M. Agostini, D.-J. Lee, B. Scrosati, Y.-K. Sun, J. Hassoun, *J. Power Sources* **2014**, *265*, 14.
[58] L. Carbone, P. T. Moro, M. Gobet, S. Munoz, M. Devany, S. G. Greenbaum, J. Hassoun, *ACS Appl. Mater. Interfaces* **2018**, *10*, 16367.
[59] G. Girishkumar, B. McCloskey, A. C. Luntz, S. Swanson, W. Wilcke, *J. Phys. Chem. Lett.* **2010**, *1*, 2193.
[60] Z. Wen, C. Shen, Y. Lu, *ChemPlusChem* **2015**, *80*, 270.
[61] J. W. Choi, D. Aurbach, *Nat. Rev. Mater.* **2016**, *1*, 1.
[62] R. Frech, W. Huang, *Macromolecules* **1995**, *28*, 1246.
[63] R. Frech, S. Chintapalli, P. G. Bruce, C. A. Vincent, *Macromolecules* **1999**, *32*, 808.
[64] S. Seki, K. Takei, H. Miyashiro, M. Watanabe, *J. Electrochem. Soc.* **2011**, *158*, A769.
[65] V. Marangon, C. Hernandez-Rentero, S. Levchenko, G. Bianchini, D. Spagnolo, A. Caballero, J. Morales, J. Hassoun, S. Cathode, *ACS Appl Energy Mater* **2020**, *3*, 12263.
[66] J. Xie, R. G. Duan, Y. Han, J. B. Kerr, *Solid State Ion* **2004**, 755–758.
[67] D. Lisbona, T. Snee, *Process Saf. Environ. Prot.* **2011**, *89*, 434.
[68] D. H. C. Wong, A. Vitale, D. Devaux, A. Taylor, A. A. Pandya, D. T. Hallinan, J. L. Thelen, S. J. Mecham, S. F. Lux, A. M. Lapides, P. R. Resnick, T. J. Meyer, R. M. Kostecki, N. P. Balsara, J. M. DeSimone, *Chem. Mater.* **2015**, *27*, 597.
[69] I. Rey, J. C. Lassègues, J. Grondin, L. Servant, *Electrochim. Acta* **1998**, *43*, 1505.
[70] K. P. Barteau, M. Wolffs, N. A. Lynd, G. H. Fredrickson, E. J. Kramer, C. J. Hawker, *Macromolecules* **2013**, *46*, 8988.
[71] T. Tamura, K. Yoshida, T. Hachida, M. Tsuchiya, M. Nakamura, Y. Kazue, N. Tachikawa, K. Dokko, M. Watanabe, *Chem. Lett.* **2010**, *39*, 753.
[72] W. A. Henderson, *J. Phys. Chem. B* **2006**, *110*, 13177.
[73] L. R. A. K. Bandara, M. A. K. L. Dissanayake, B.-E. Mellander, *Electrochim. Acta* **1998**, *43*, 1447.
[74] M. E. F. de Ruiz Holgado, C. R. de Schaefer, E. L. Arancibia, *J. Chem. Eng. Data* **2002**, *47*, 144.
[75] G. B. Appetecchi, F. Croce, L. Persi, F. Ronci, B. Scrosati, *Electrochim. Acta* **2000**, *45*, 1481.
[76] R. Kido, K. Ueno, K. Iwata, Y. Kitazawa, S. Imaizumi, T. Mandai, K. Dokko, M. Watanabe, *Electrochim. Acta* **2015**, *175*, 5.
[77] Y. Ma, *J. Electrochem. Soc.* **1995**, *142*, 1859.
[78] T. Sakakibara, M. Kitamura, T. Honma, H. Kohno, T. Uno, M. Kubo, N. Imanishi, Y. Takeda, T. Itoh, *Electrochim. Acta* **2019**, *296*, 1018.
[79] C. Wang, T. Deng, X. Fan, M. Zheng, R. Yu, Q. Lu, H. Duan, H. Huang, C. Wang, X. Sun, *Joule* **2022**, *6*, 1770.
[80] B. W. Zewde, S. Admassie, J. Zimmermann, C. S. Isfort, B. Scrosati, J. Hassoun, *ChemSusChem* **2013**, *6*, 1400.
[81] N. Imanishi, A. C. Luntz, P. Bruce, *The Lithium Air Battery*, Springer, New York, **2014**, pp. 1–334.
[82] A. Débart, J. Bao, G. Armstrong, P. G. Bruce, *J. Power Sources* **2007**, *174*, 1177.
[83] Z. Peng, S. A. Freunberger, Y. Chen, P. G. Bruce, *Science* **2012**, *337*, 563.
[84] M. M. Ottakam Thotiyl, S. A. Freunberger, Z. Peng, P. G. Bruce, *J. Am. Chem. Soc.* **2013**, *135*, 494.
[85] W.-J. Kwak, Rosy, D. Sharon, C. Xia, H. Kim, L. R. Johnson, P. G. Bruce, L. F. Nazar, Y.-K. Sun, A. A. Frimer, M. Noked, S. A. Freunberger, D. Aurbach, *Chem. Rev.* **2020**, *120*, 6626.

Manuscript received: April 28, 2023
Accepted manuscript online: May 19, 2023
Version of record online: July 12, 2023

© 2023 The Authors. Chemistry - A European Journal published by Wiley-VCH GmbH

15213765, 2023, 45, Downloaded from https://chemistry-europe.onlinelibrary.wiley.com/doi/10.1002/chem.202301345 by Universita Di Ferrara, Wiley Online Library on [08/10/2024]. See the Terms and Conditions (https://onlinelibrary.wiley.com/terms-and-conditions) on Wiley Online Library for rules of use; OA articles are governed by the applicable Creative Commons License